frontiers in Immunology

ORIGINAL RESEARCH
published: 29 September 2020
doi: 10.3389/fimmu.2020.529219

Th1-Dependent *Cryptococcus*-Associated Immune Reconstitution Inflammatory Syndrome Model With Brain Damage

Yee Ming Khaw[1,2], Nupur Aggarwal[3], William E. Barclay[3], Eunjoo Kang[1,2], Makoto Inoue[1,2] and Mari L. Shinohara[3,4]**

[1] Department of Comparative Biosciences, University of Illinois at Urbana-Champaign, Urbana, IL, United States, [2] Neuroscience Program, University of Illinois at Urbana-Champaign, Urbana, IL, United States, [3] Department of Immunology, Duke University School of Medicine, Durham, NC, United States, [4] Department of Molecular Genetics and Microbiology, Duke University School of Medicine, Durham, NC, United States

OPEN ACCESS

Edited by:
Markus M. Heimesaat, Charité – Universitätsmedizin Berlin, Germany

Reviewed by:
Camaron Hole, Washington University School of Medicine in St. Louis, United States
Wendy Szymczak, Montefiore Medical Center, United States

***Correspondence:**
Makoto Inoue
makotoi@illinois.edu
Mari L. Shinohara
mari.shinohara@duke.edu

Specialty section:
This article was submitted to Microbial Immunology, a section of the journal Frontiers in Immunology

Received: 23 January 2020
Accepted: 04 September 2020
Published: 29 September 2020

Citation:
Khaw YM, Aggarwal N, Barclay WE, Kang E, Inoue M and Shinohara ML (2020) Th1-Dependent Cryptococcus-Associated Immune Reconstitution Inflammatory Syndrome Model With Brain Damage. Front. Immunol. 11:529219. doi: 10.3389/fimmu.2020.529219

Cryptococcus-associated immune reconstitution inflammatory syndrome (C-IRIS) is identified upon immune reconstitution in immunocompromised patients, who have previously contracted an infection of *Cryptococcus neoformans* (*Cn*). C-IRIS can be lethal but how the immune system triggers life-threatening outcomes in patients is still poorly understood. Here, we establish a mouse model for C-IRIS with *Cn* serotype A strain H99, which is highly virulent and the most intensively studied. C-IRIS in mice is induced by the adoptive transfer of $CD4^+$ T cells in immunocompromised *Rag1*-deficient mice infected with a low inoculum of *Cn.* The mice with C-IRIS exhibit symptoms which mimic clinical presentations of C-IRIS. This C-IRIS model is Th1-dependent and shows host mortality. This model is characterized with minimal lung injury, but infiltration of Th1 cells in the brain. C-IRIS mice also exhibited brain swelling with resemblance to edema and upregulation of aquaporin-4, a critical protein that regulates water flux in the brain in a Th1-dependent fashion. Our C-IRIS model may be used to advance our understanding of the paradoxical inflammatory phenomenon of C-IRIS in the context of neuroinflammation.

Keywords: immune reconstitution inflammatory syndrome, *Cryptococcus neoformans*, interferon-γ, aquaporin-4, Th1 cells, astrocytes, neuroinflammation

INTRODUCTION

Immune reconstitution inflammatory syndrome (IRIS) is a pathological condition whereby a recovering immune system paradoxically worsens the patient's condition by responding excessively to a previously acquired infection (1, 2). IRIS has been reported in patients, who are recovering from an immunocompromised condition and pre-infected with fungi such as *Cryptococcus, Candida, Aspergillus*, as well as mycobacteria and viruses (3–5). Among these, *Cryptococcus*-associated IRIS (hereinafter "C-IRIS") is one of the most prevalent IRIS subtypes, and is reported to cause rapid wasting and mortality in immunocompromised patients after immune reconstitution (4, 6–8). Approximately 25% of HIV-infected patients who underwent antiretroviral therapy (6, 9, 10) and ∼5% of immunocompromised patients who had received a solid-organ transplant develop C-IRIS

(11). A meta-analysis showed that while lethality was 4.5% for all types of IRIS conditions, lethality for C-IRIS was shown to be 20.8% (8). Not only in AIDS patients, C-IRIS is also reported in some multiple sclerosis (MS) patients. These MS patients had *Cryptococcus* infection prior to discontinuing Natalizumab treatment (12). Natalizumab is an integrin α4 antibody, which prevents T cell migration into the central nervous system (CNS). Therefore, cessation of Natalizumab treatment is considered to allow T cell influx to the CNS. These observations suggest that the history of *Cryptococcus* infection before the influx of $CD4^+$ T cells to the CNS may be a crucial feature of C-IRIS induction. Interestingly, C-IRIS also manifests in postpartum women (13, 14). During pregnancy, increased estrogen suppresses the immune system (15) and makes the host vulnerable to fungal infections (16). In the postpartum phase, the immune system is reactivated upon normalization of the estrogen levels, thus triggering C-IRIS development (17). Collectively, these reports suggest that clinical conditions typified by a rapid immune recovery are conducive to the development of C-IRIS.

The $CD4^+$ T cell is a key player in driving C-IRIS disease development (18, 19). Patients with C-IRIS typically present with a high number of circulating $CD4^+$ T cells, particularly of the Th1 subtype, as well as upregulation of pro-inflammatory cytokine production coupled with clinical pathologies of pulmonary dysfunction, CNS lesions, and brain edema (6–8, 20). Exuberant secretion of cytokines, or a 'cytokine storm,' is proposed to underlie C-IRIS (21). However, cytokine levels in the cerebrospinal fluid at the time of C-IRIS is similar to those during initial *Cryptococcus* meningitis among non-C-IRIS patients (7, 22), suggesting an alternative mechanism, rather than cytokine storm, to explain the CNS symptoms of C-IRIS.

Currently, NSAIDs (nonsteroidal anti-inflammatory drugs) and corticosteroids are prescribed to suppress excessive inflammation in C-IRIS patients (5), but such immunosuppressive treatments may impair a response to the existing infection and increase susceptibility to new infections (23, 24). The lack of effective treatments for C-IRIS stems, at least in part, from poor understanding of C-IRIS pathogenesis. To understand the C-IRIS pathogenesis, an animal model which accurately represents the human condition of C-IRIS is essential.

To that end, we report a mouse model for C-IRIS using *Cn* serotype A, which is widespread in the environment (25) and the most commonly identified in HIV patients (26–28). This mouse model presents phenotypes similar to human C-IRIS symptoms, such as systemic upregulation of some inflammatory cytokines and brain edema. Our finding addresses the urgent need for a model to investigate specific cellular and molecular mechanisms underlying C-IRIS.

MATERIALS AND METHODS

Mice

Rag1$^{-/-}$ (JAX 002216) and *Ifng*$^{-/-}$ (JAX 008228) mice of the C57BL/6J background and C57BL/6J (JAX 000664) mice were purchased from The Jackson Laboratory. Mice were kept under specific pathogen-free conditions with a 12-h light/dark cycle. Sterile food and water were given *ad libitum* in concordance with the recommendations for the health monitoring of mice. Healthy male and female mice aged 16–20 weeks were randomly selected for use in this study. No sex-specific outcomes were observed. The study was performed under approvals of the Duke University Institutional Animal Care and Use Committee (protocol number A088-18-04) and University of Illinois Institutional Animal Care and Use Committee (protocol number 19171).

C-IRIS Induction

*Cn*H99 was cultured on YPD (yeast extract 1%, peptone 2%, and dextrose 2%) plates or YPD liquid medium at 30°C with 150 rpm shaking overnight (29). Protocol optimization brought the following methods to be the most reproducible and clinically relevant: *Rag1*$^{-/-}$ mice of 16–20 weeks old were intranasally infected with *Cn*H99 (100 yeasts in 30 μl PBS). $CD4^+$ T cells were intravenously transferred (10^6 cells in 200 μl PBS with 2% FBS) into *Cn*H99 pre-infected mice 3 weeks after *Cn*H99 infection, unless otherwise noted. The C-IRIS experiment scheme with three control groups (naïve, infection alone, T cell transfer alone) is presented in the **Supplementary Figure 1A**. $CD4^+$ T cells were isolated from the spleen and inguinal/axillary lymph nodes of naïve C57BL6 mice (6–8 weeks old) and enriched by negative selection using microbeads (STEMCELL, $CD4^+$ cells enrichment). The purity of isolated $CD4^+$ T cells was 90–95%. Enriched $CD4^+$ T cells included 70.5% naïve ($CD62L^+CD44^-$), 11.3% central memory ($CD62L^+CD44^{hi}$), 13.2% effector ($CD62L^-CD44^{hi}$) $CD4^+$ T cells ($n = 3$ average), and 9.1% of Treg cells ($CD3^+CD4^+Foxp3^+$). Mice were monitored daily, and body weights were recorded.

ELISA for Serum and Brain Cytokine Levels

Serum and brain cytokine concentrations (IL-6, IL-1β, TNFα, and/or IFNγ) were evaluated using ELISA kits (R&D; DY406 for IL-6, DY401 for IL-1β, DY410 for TNFα, DY823405 for IFNγ). For brain cytokine analysis, the hindbrain region (Bregma −5.0 to −8.0 mm) was dissected with a clean blade and added ice-cold 300 μl RIPA buffer (Fisher Scientific, PI89901) with Halt™ Protease Inhibitor Cocktail (Fisher Scientific, PI78425). Tissues were homogenized and centrifuged for 20 min at 13,000 rpm at 4°C. Protein concentrations were evaluated by the BCA protein quantitation (Fisher Scientific, 23227). All ELISA assays were performed as suggested by manufactures' instructions.

Evaluation of Fungal Burdens

Mice were euthanized by CO_2 inhalation, and lung and brain were removed. For the enumeration of fungal load, organs were homogenized in 1 mL PBS. Serial dilutions of the homogenates were plated on YPD plates and incubated for 48 h at 30°C to evaluate colony-forming units (CFU).

Leukocytes Isolation From the Brain and Lung

To prepare cells from the lung and brain, tissues were excised and minced in PBS supplemented with collagenase D

(1 mg/ml). Minced tissues were incubated for 30 min at 37°C, filtered through 80-μm mesh, then centrifuged at 4°C. We performed hemolysis for cells obtained from the lung. To isolate mononuclear cells from brain and lungs, cells were resuspended in 30% Percoll (in PBS) laid over 70% Percoll, and centrifuged for 20 min at room temperature.

Cell Staining for Flow Cytometry and Analyses

Before cell staining with antibodies, Fc receptors were blocked with Fc Block (BD Pharmingen) for 7 min on ice. Cells were stained with fluorochrome-conjugated specific antibodies for 30 min on ice, washed, fixed with 4% paraformaldehyde, and analyzed by flow cytometry within 24 h. For intracellular cytokine staining, cells were treated with PMA (10 ng/ml) and Ionomycin (1 μg/ml) for 4 h, including the BD GolgiPlug™ Protein Transport Inhibitor (BD Biosciences BD 555029) treatment in the last 2 h. Cell surface markers were stained first, then intracellular cytokine staining was performed with Cytofix/Cytoperm kit (BD Biosciences; to stain IFN-γ and IL-17) and FOXP3 Fix/Perm Kit (BioLegend; to stain Foxp3). LIVE/DEAD™ fixable dead cell stain kit (Invitrogen) was used to gate out dead cells. Antibodies for flow cytometry are listed in **Supplementary Table 1**. Flow cytometry data were collected with Cytek Aurora or FACS Canto II (BD) and analyzed with the FlowJo software (Treestar) or FCS Express (De Novo). In lung-derived leukocytes, DC or interstitial or exudate macrophages (DC/iMΦ/eMΦ) were identified as $CD45^+CD11c^+F4/80^-$, alveolar macrophages (AM) as $CD45^+CD11c^+F4/80^+$, inflammatory macrophage/monocyte as $CD45^+Ly6C^+CD11b^+$, neutrophils as $CD45^+Ly6G^{hi}CD11b^+$, and $CD4^+$ T cells as $CD45^+CD3^+CD4^+$. Gating strategy for lung myeloid cells in the lung is provided in **Supplementary Figure 1C**. In brain-derived leukocytes, $CD4^+$ T cells were identified as $CD45^+CD3^+CD4^+$, microglia as $CD45^{lo}F4/80^+$, macrophage as $CD45^{hi}F4/80^+$, and neutrophils as $CD45^+Ly6G^+$. Gating strategy to separate microglia from infiltrated macrophages/monocytes is shown in **Supplementary Figure 3A**. Representative flow cytometry results detecting intracellular IFNγ, IL-17, and Foxp3 in brain-infiltrated $CD4^+$ T cells are found in **Supplementary Figure 3B**.

Histology of the Lung and Brain, and Quantitative Evaluation of Images

Organs were harvested after perfusion with 4% paraformaldehyde in PBS and embedded into paraffin blocks. Tissue slices (10 μm) were stained with 0.1% Mayer's Hematoxylin (H&E) for 20 min, rinsed in cool running ddH_2O for 5 min, then stained with Eosin (0.5% in 95% EtOH) for 12 s. H&E images were acquired using a brightfield microscope with 4× objective. "Area of distal airspaces as percentage (%) of total distal lung area" was evaluated as described in a previous study (30) using ImageJ by manually outlining the areas using a wand tool. Brain vacuolization areas were analyzed with a similar quantitative approach. One data point/mouse in quantitation of histological images is an average value of at least 16 fields (>2 fields/section, 8 sections/mouse) for the lung and at least 3 fields (>3 sections/mouse) for the brain. At least 3 mice/group were used for lung H&E. At least 5 mice/group were used for brain H&E.

Quantitative Evaluation of Brain Edema

To evaluate brain edema (swelling), circumferences of midbrain (around bregma −1.9 mm) and hindbrain (around bregma −6.3 mm) were measured with manufactured silk and ruler with 0.1 mm accuracy. To minimize variation in measurement, a single person performed the process, and used average values from repeated measurement per sample.

AQP4 Immunohistochemistry

Brains were perfused, fixed overnight in 4% paraformaldehyde, and cryoprotected by a 30% sucrose treatment in ddH_2O, before being frozen in the OCT compound (Sakura, Japan). Coronal tissue slices (30 μm) were stained with AQP4 antibody (Novus, 1:500) and goat anti-rabbit Alexa-488 secondary antibody (1:500). Product information of antibodies is listed in **Supplementary Table 1**. Image fields of superior part of the brainstem (bregma −5.80 mm – bregma −6.24) were acquired by a fluorescent microscope (Leica DM 2000, IL, United States). AQP4 expression was quantified as the area stained with AQP4 antibody over total area with the ImageJ software by converting images to gray scale and being analyzed with the "thresholding" approach[1]. All were blinded during the assessment, and at least four sections of brain stem of each animal (n = *3–5*/group) were evaluated by one individual.

Astrocyte Cell Line Culture

Mouse astrocyte cell line C8-D30 (ATCC, CRL-2534; 10^6 cell/well) was seeded in 24-well plates. One day after seeding, rIFNγ, rIL-17, rIL-6, rIL-1β (10 ng/ml each), or *Cn*H99 (10^7 yeasts/well) were added to cell culture, and cells were incubated for 5 h at 37°C. Cells were used for RT-qPCR.

RNA and cDNA Preparation for Standard qPCR Analyses

Total RNA was extracted from cells with RNeasy Kit (Qiagen). cDNA synthesis was performed with qScript cDNA SuperMix (Quanta). qPCR analysis was performed with KAPA-SYBR-FAST (KAPA BioSystems) with an initial denaturing step at 95°C for 3 min, followed by 35 cycles of a denaturation step (94°C for 3 s) and an annealing/extension step (60°C for 30 s). The relative amounts of qPCR products were determined with the $\Delta\Delta Ct$ method with *Actb* (β-actin) as an internal control. Primers are listed in **Supplementary Table 2**.

Statistical Evaluations

Sample sizes, numbers of animals, and factors used for statistical evaluations are indicated in figure legends and this Methods section. Student's *t*-test (two-tailed, if not indicated otherwise) was performed for two group comparison. In case of comparisons of multiple groups, one-way ANOVA and the Tukey *post-hoc* test were performed. Log-rank analysis were used to

[1]https://imagej.net/Thresholding

statistically evaluate survival curve data. *P*-values of 0.05 or less were considered statistically significant. Statistical analyses and graphical presentations were computed with GraphPad Prism software (GraphPad, La Jolla, United States).

RESULTS

Experimental C-IRIS Condition Results in Clinical Manifestations of Weight Loss and Death

Cryptococcus-associated immune reconstitution inflammatory syndrome is a complex disorder with high mortality risk in a significant proportion of immunocompromised persons with a history of cryptococcosis (6). To mimic clinical symptoms of C-IRIS, *Rag1*$^{-/-}$ mice were reconstituted with CD4$^+$ T cells (10^6 cells/mouse) by adoptive transfer 3 weeks after infection with *Cryptococcus neoformans* serotype A H99 (CnH99, 100 yeasts/mouse) (**Supplementary Figure 1A**), unless otherwise noted. While control mice (CnH99-infection alone) did not lose weights between week 3 and 4, 80% of C-IRIS mice (CnH99 + CD4$^+$ T) approached the humane endpoint (∼30% weight loss) within 12 days after T cell transfer (**Figure 1A**). Only 20% of C-IRIS mice survived beyond 10 days after T cell transfer. In contrast, all control mice survived (naïve, CnH99-infection alone, and CD4$^+$ T cell transfer alone) in the experiment period (**Figure 1B**). Interestingly, adoptive transfer of CD8$^+$ T cells (10^6 cells/mouse) did not induce mortality (**Figure 1B**), emphasizing that the pathogenic role is specific to CD4$^+$ T cells in C-IRIS. Next, we examined if the period of *Cn* infection before T cell transfer affects C-IRIS severity. Mice pre-infected with CnH99 for 2 weeks before CD4$^+$ T cell transfer had significantly greater survival compared to mice with pre-infection period of 3 or 4 weeks (**Figure 1C**). These results indicate that C-IRIS mortality is induced specifically by CD4$^+$ T cells and that the C-IRIS becomes more severe with extended periods of *Cn* infection.

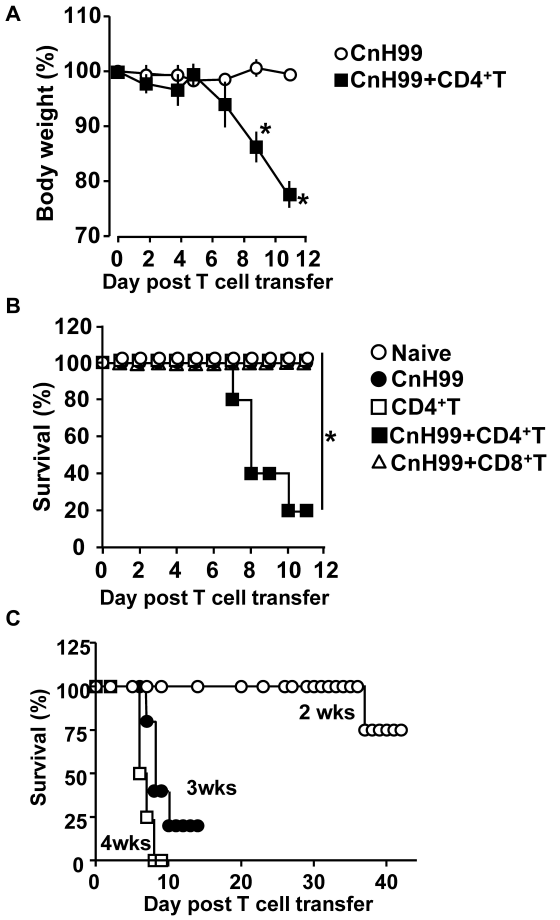

FIGURE 1 | Weight loss and mortality with C-IRIS. **(A)** Comparison of mouse body weights between groups that had infection alone (CnH99) vs. C-IRIS (CnH99 + CD4$^+$ T). CnH99 (100 yeasts/mouse) was intranasally infected 3 weeks before CD4$^+$ T cell transfer. **(B)** Mouse survival comparing five groups; 4 groups with the protocol indicated in **Supplementary Figure 1A**, and another group with CnH99 infection and CD8$^+$ T cell transfer. Log-rank analysis were used for statistical evaluation. **(C)** C-IRIS mouse survival to evaluate the *Cn*H99 infection period before CD4$^+$ T cell transfer. Infection periods tested are 2 weeks (○), 3 weeks (●), and 4 weeks (□). *n = 5–10* mice per group for all experiments. Results are representatives of at least two independent experiments; $^*p < 0.05$.

C-IRIS Heightens Serum Levels of Some Inflammatory Cytokines

In human C-IRIS, pro-inflammatory cytokine levels in serum increase dramatically after immune reconstitution (7, 31, 32). To assess systemic cytokine levels in our C-IRIS model, we examined four major pro-inflammatory cytokines in sera from C-IRIS mice with three control conditions (naïve, CnH99-infection alone, and CD4$^+$ T cell transfer alone). C-IRIS mice showed significantly higher concentrations of TNFα and IL-6 in serum than control mice, while no notable differences were observed in IL-1β and IFNγ concentrations (**Figure 2**). The result indicates the systemic upregulation of specific inflammatory cytokines in C-IRIS.

C-IRIS Enhances Lung Myeloid Cell Counts but Not Lung Fungal Burden

We first examined the lung fungal burden in CnH99-infected *Rag1*$^{-/-}$ mice without T cell transfer. Fungal burden steadily increased over 3 weeks after CnH99 infection and accelerated after week 3 (**Figure 3A**). Without T cell transfer, an increase in fungal burden was also found in the spleen but not as drastic as that observed in the lung (**Supplementary Figure 1B**). A previous report showed that a major risk factor in C-IRIS is high *Cn* burden in the lungs and the CNS (33). However, no difference in lung fungal loads was observed between groups with C-IRIS vs. infection alone at 4 weeks post infection (IRIS group had T cell transfer 7 days before the analysis) (**Figure 3B**). The result suggested that lung fungal loads do not explain the mortality of IRIS mice.

Next, we investigated numbers of major cell subtypes in the lung. The low infection inoculum in our protocol did not

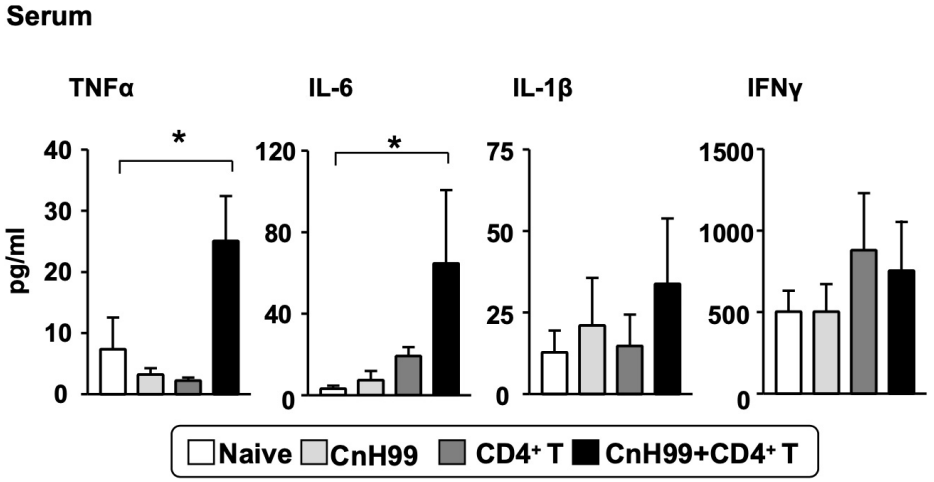

FIGURE 2 | Serum proinflammatory cytokine levels. Serum cytokine levels of TNF-α, IL-6, IL-1β, and IFNγ were compared among 4 groups of mice with the protocol as indicated in **Supplementary Figure 1A**. Serum samples were obtained 4 weeks after *Cn* infection. C-IRIS received $CD4^+$ T cell transfer 3 weeks after infection. $n = 5$ mice per group for all experiments. The results are representatives from two independent experiments. One-way ANOVA and Tukey *post-hoc* test were used for statistical analyses; $^*p < 0.05$.

increase cell numbers of various myeloid cells without T cell transfer (**Figure 3C**). However, increased numbers of myeloid cells were observed in lungs of C-IRIS mice, compared to lungs of control groups (**Figure 3D**). These results suggest that C-IRIS does not increase lung fungal burdens, but enhances myeloid cell recruitment in the lung.

Pathogenic Role of Th1 Cells in C-IRIS

C-IRIS mice had significantly more $CD4^+$ T cells in the lungs than mice subjected to T cell transfer alone 7 days after T cell transfer (**Figure 4A**). Because the two groups received the same number of $CD4^+$ T cells, the result suggested the significant increase of T cells in C-IRIS mice is involved in the pathology. To understand the potential mechanism, we evaluated the expression of T cell co-stimulatory molecule in $CD45^+CD11c^+F4/80^-$ antigen-presenting cells (APCs), mainly dendritic cells (DCs). Among the eight co-stimulatory molecules examined, APCs in C-IRIS mice showed increased expressions of CD40 and 4-1BBL, although no significant difference was found in CD357, B7H2, Ox42L, CD70, CD80, and CD86 (**Figure 4B**). $CD4^+$ T cells in C-IRIS mice also significantly increased the expression of CD40L, a CD40 ligand (**Figure 4C**). These results suggest an enhanced CD40-CD40L interaction between APCs and $CD4^+$ T cells in the lung during C-IRIS. We also found that a majority of lung-infiltrated T helper cells in C-IRIS mice are Th1 cells (**Figure 4D**), similar to the lung in human C-IRIS (34, 35). To determine if our C-IRIS model is driven by Th1 cells, we transferred *Ifng*$^{-/-}$ $CD4^+$ T cells into CnH99 pre-infected *Rag1*$^{-/-}$ mice and monitored their survival. C-IRIS-induced mice with *Ifng*$^{-/-}$ $CD4^+$ T cells indeed survived significantly longer than those with IFNγ-sufficient $CD4^+$ T cells (**Figure 4E**). This result strongly suggests the involvement of Th1 cells in the pathogenicity of our C-IRIS model.

C-IRIS Impacts the Brain More Than the Lung

Fungal burden and leukocyte accumulation in the lung of C-IRIS mice led us to suspect lung damage as a cause for mortality. However, unexpectedly, C-IRIS mice did not exhibit significant histopathology in the lung (**Figure 5A**). Since it was difficult to tell histological differences by eye, we quantitatively evaluated the air sac areas in the histology images (**Figure 5B**). Nevertheless, C-IRIS mice still did not show abnormality and kept shapes of alveoli as well as other groups. Because our analyses suggest no abnormalities in the lung histology, we examined the brain. CnH99 is known to enter the brain via direct transmigration of the capillary endothelium or infected phagocytic cells (36). Before T cell transfer, no fungal burden was detected in the first 3 weeks but exponentially increased at week 4 (**Figure 6A**). However, we again found no difference in brain fungal loads between IRIS mice and CnH99-infected control mice without T cell transfer 7 days after C-IRIS mice received T cell transfer (**Figure 6B**). Because C-IRIS is often characterized by CNS inflammation, we enumerated leukocyte infiltrates and CNS-resident microglia in the C-IRIS brain. Although control groups (naïve, CnH99-infection alone, T cell transfer alone) did not show signs of inflammatory cell infiltration in the brain, C-IRIS mice showed clear infiltration of $CD4^+$ T cells, macrophages/monocyte, and neutrophils, as well as increased numbers of microglia (**Figure 6C**). Additionally, a majority of brain-infiltrated T helper cells were Th1 cells in C-IRIS mice (**Figure 6D**).

Gross phenotypical changes in the brain, such as edema was observed in C-IRIS mice 7 days after $CD4^+$ T cell transfer but not in control cohorts (**Figure 7A**). The phenotype in C-IRIS mice was particularly significant in hindbrain, rather than midbrain (**Figure 7B**). Importantly, no increase of hindbrain circumference was observed when C-IRIS was induced with *Ifng*$^{-/-}$ $CD4^+$ T cells (**Figures 7A,B**). Tissue damage, identified with extra void

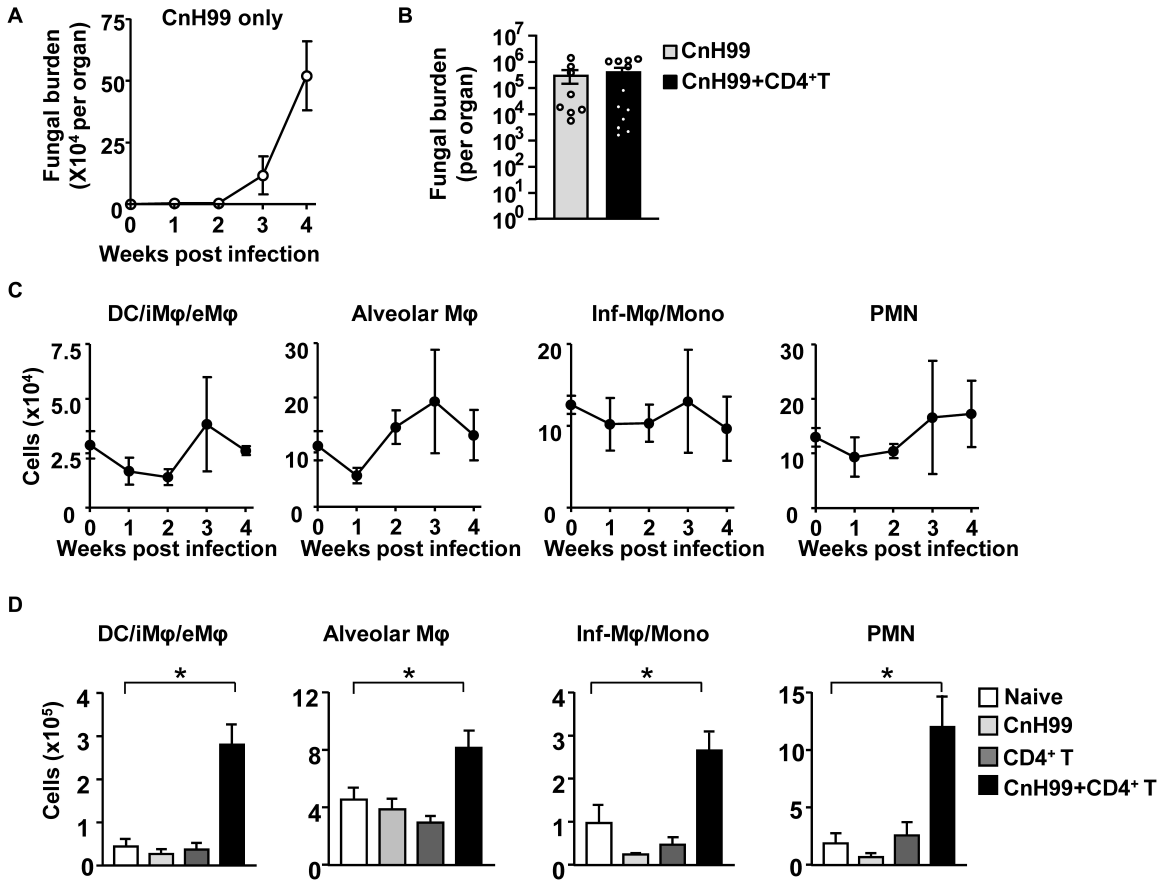

FIGURE 3 | Fungal burdens and numbers of immune cells in the lung. **(A)** Lung fungal loads at indicated time-points (0, 1, 2, 3, and 4 weeks) post infection in a group with infection alone. **(B)** Comparison of lung fungal loads between mice with fungal infection alone (CnH99) and C-IRIS (CnH99 + $CD4^+$ T cells) with the protocol indicated in **Supplementary Figure 1A**. One data-point denotes a result from one mouse. **(C,D)** Cell numbers of indicated myeloid cell types in the lung. Time-course data of a group with infection alone **(C)**. Comparison among 4 groups with the C-IRIS protocol indicated in **Supplementary Figure 1A** at 4 weeks after infection **(D)**. Flow cytometry was used for the analyses by determining DC, interstitial, and exudate macrophages (DC/iMΦ/eMΦ) as $CD45^+CD11c^+F4/80^-$, alveolar macrophages (AM) as $CD45^+CD11c^+F4/80^+$, inflammatory macrophage/monocyte as $CD45^+Ly6C^+CD11b^+$, and neutrophils as $CD45^+Ly6G^{high}CD11b^+$. *n = 5* mice per group for all experiments, except for **(B)**. The results are representatives from at least two independent experiments. One-way ANOVA and Tukey *post-hoc* test were used for statistical analyses; $^*p < 0.05$.

spaces and vacuolization, were observed in hindbrain of C-IRIS mice 7 days after $CD4^+$ T cell transfer (**Figures 7C,D**). Notably, tissue damage was also observed in C-IRIS-induced mice with *Ifng*$^{-/-}$ $CD4^+$ T cells, but to a lesser extent in mice with infection only (**Figures 7C,D**). We found that expression of AQP4, a main contributor to brain fluid homeostasis, was upregulated in the hindbrain of C-IRIS mice, while no AQP4 upregulation was observed in C-IRIS-induced mice with *Ifng*$^{-/-}$ $CD4^+$ T cells (**Figures 7E,F**). Previous studies demonstrated that transcription of *Aqp4* in astrocytes is upregulated by inflammatory cytokines (37, 38). Thus, we evaluated *Aqp4* gene expression by treating the C8-30 astrocyte cell line with recombinant (r) IFNγ, rIL-17, rIL-6, rIL-1β, or CnH99 for 5 h. *Aqp4* mRNA levels were significantly upregulated with IFNγ but not with other treatment conditions (**Figure 7G**). Although the behavior of astrocytes *in vivo* cannot be replicated by cell line experiments, the result at least suggested *Aqp4* expression in astrocytes can be induced by IFNγ. Therefore, we evaluated IFNγ levels in the hindbrain and found that C-IRIS mice showed elevated IFNγ protein levels in the hindbrain (**Figure 7H**). In sum, these results suggest that C-IRIS induces brain damage with edema characterized by enhanced IFNγ and *Aqp4* expression in the hindbrain.

DISCUSSION

Patients with C-IRIS present high $CD4^+$ T cell numbers, particularly Th1 cells (6, 8), suggesting a crucial role for Th1 in C-IRIS development. A previous study of a C-IRIS mouse model used the less virulent *Cn* serotype D, 1841 strain and reported that C-IRIS is Th1-independent (39). The 1841 strain was originally isolated from human patients (40), as well as H99 (41). The 1841 C-IRIS model showed mild weight loss up to 6–7% with no mortality (39), possibly due to the low virulence of the strain. Therefore, the impact of Th1 cells may not have

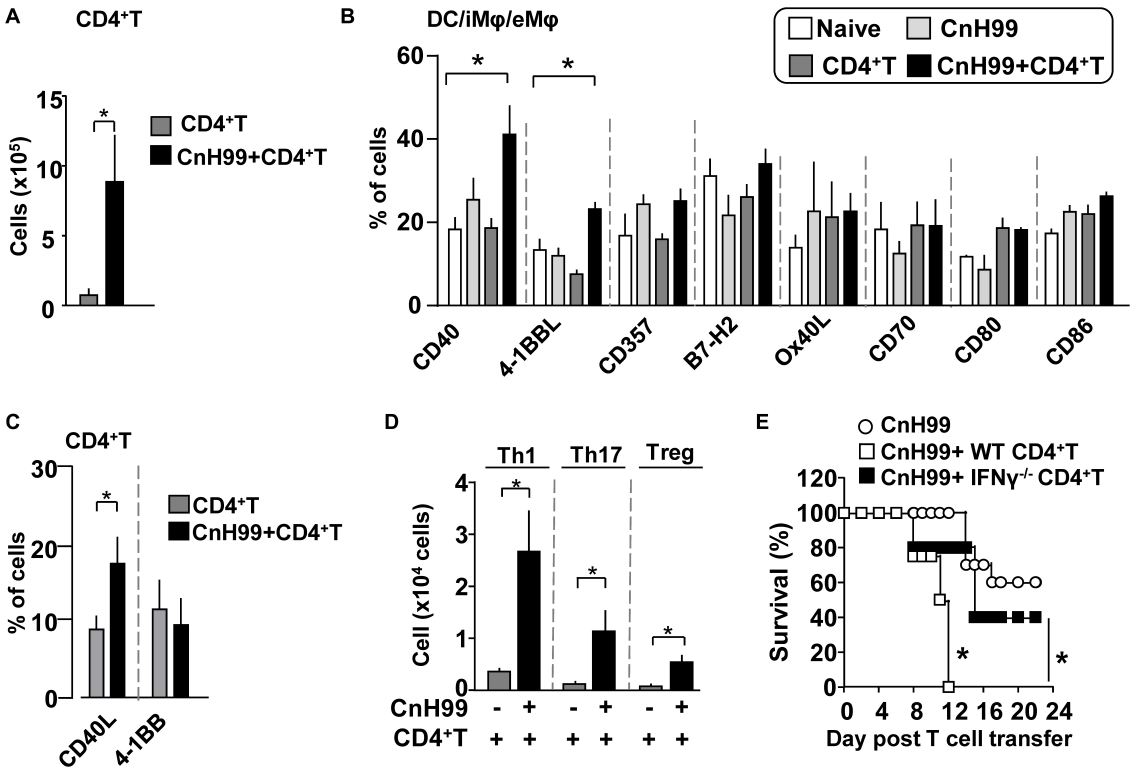

FIGURE 4 | Evaluation of $CD4^+$ T cells and APCs in C-IRIS. **(A)** Comparison of lung $CD4^+$ T cell counts between groups with C-IRIS vs. T cell transfer alone. **(B)** Expression of co-stimulatory molecules on $CD45^+CD11c^+F4/80^-$ cells. **(C,D)** Percentages of $CD4^+$ T cells expressing CD40L or 4-1BB **(C)**. Numbers of Th1, Th17, and Treg cells in the lung **(D)**. **(E)** Survival C-IRIS-induced mice with *Ifng*$^{-/-}$ $CD4^+$ T cell or wild type $CD4^+$ T cell. A control group with infection alone received vehicle (PBS with 2% FBS) injection at the same time with T cell transfer for test groups. Day 0 was set 3 weeks after infection. Except for **(E)**, evaluations were performed at 4 weeks post infection and/or 1 week after T cell transfer, and the treatment protocol of groups is indicated in **Supplementary Figure 1A**. *n = 5* mice per group for all experiments. The results are representatives from at least two independent experiments. Student's *t*-test for **(A,C,D)**, one-way ANOVA and Tukey *post-hoc* test for **(B)**, and Log-rank analysis for **(E)** were used for statistical analyses; $^*p < 0.05$.

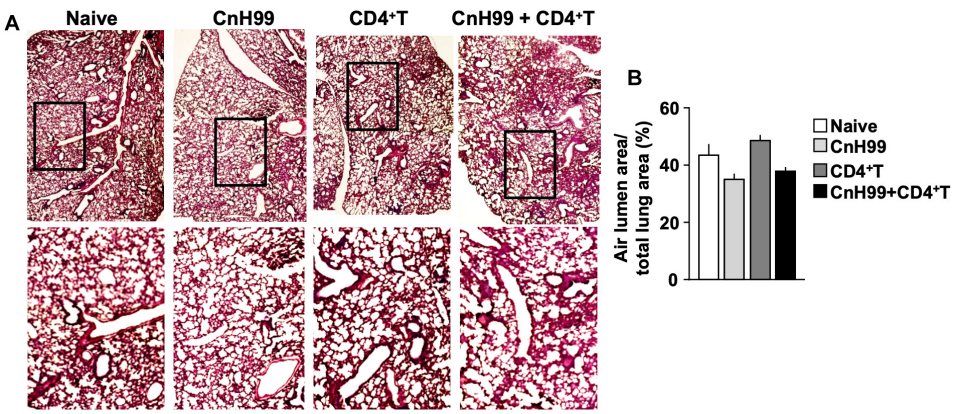

FIGURE 5 | Evaluating lung pathology in C-IRIS mice. **(A)** Representative images of H&E-stained lungs collected from 4 groups with the protocol, indicated in **Supplementary Figure 1A**. **(B)** Quantitative analysis of areas of distal airspaces in lung sections, calculated from average values of at least 16 fields/mouse (more details are described in the section "Materials and Methods"); *n > 3* mice/group. The results are representatives from two independent experiments.

been clear in the hosts. In contrast, our model employs the highly virulent *Cn* serotype A, H99 strain. Unlike the 1841 C-IRIS model, our H99 C-IRIS model demonstrates rapid wasting and mortality, as well as Th1 responses, thus capturing the phenotype of dramatic deterioration and death as seen in some C-IRIS patients (4, 6, 7).

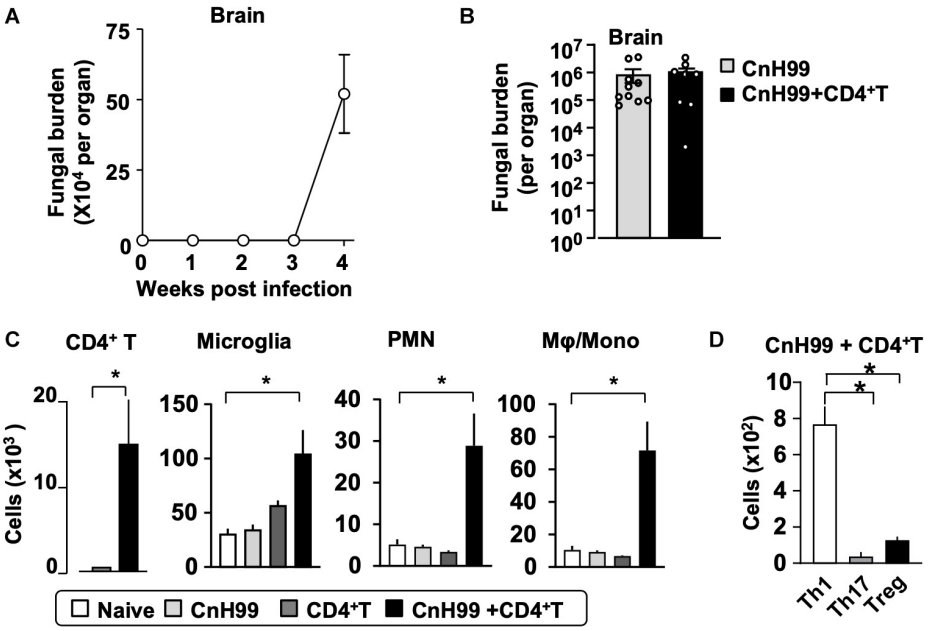

FIGURE 6 | CNS fungal burden and immune cell infiltration. **(A)** Time-course of fungal loads in brains after CnH99 infection in a group with infection alone. **(B)** Comparison of brain fungal loads between mice with infection alone (CnH99) vs. C-IRIS (CnH99+CD4$^+$ T cells). One data-point denotes a result from one mouse. **(C)** Numbers of indicated cell types in the brain of mice among four groups of mice. **(D)** Numbers of infiltrated Th1 (CD45$^+$CD3$^+$CD4$^+$IFNγ$^+$), Th17 (CD45$^+$CD3$^+$CD4$^+$IL17$^+$), Treg (CD45$^+$CD3$^+$CD4$^+$Foxp3$^+$) in the brain of C-IRIS mouse. Gating strategy for each cell type is shown in **Supplementary Figure 3B**. Except for **(A)**, evaluations were performed at 4 weeks post infection and/or 1 week after T cell transfer, and the treatment protocol of groups is indicated in **Supplementary Figure 1A**. *n = 5* mice/group for all experiments. The results are representatives from two independent experiments. Student's *t*-test (**C**; CD4$^+$ T cells) and one-way ANOVA and Tukey *post-hoc* test for (**C**; myeloid cells, **D**) were used for statistical analyses; $^*p < 0.05$.

We asked if the pathogenicity of C-IRIS is attributed to possible systemic increase of proinflammatory cytokine levels. C-IRIS mice indeed showed enhanced cytokine levels but the levels are much lower than those seen in mice with LPS endotoxemia. For example, serum TNF-α levels in mice with LPS endotoxemia rise to 1,000–8,000 pg/ml (42), while C-IRIS mice had ∼25 pg/ml of blood TNF-α, as shown in **Figure 2**. Thus, the relatively mild increase of serum proinflammatory cytokines in C-IRIS mice does not appear to be significant enough to explain the acute death of the mice (**Figure 1B**).

Next, we speculated if the pathogenicity of C-IRIS results from lung injury triggered by lung inflammation and damage. First, numbers of lung infiltrated myeloid cells kept low without significant changes without T cell transfer. One possibility for this is the low inocula and immunogenicity of *Cn,* encapsulated for evasion from host detection (43). Our histology data also indicated minimal lung injury in C-IRIS mice, despite cellular infiltration including macrophages, neutrophils, and dendritic cells in the lung. In contrast to *Cn*, it is of note that *Mycobacterium avium* elicits strong innate immune responses and was used in a *Mycobacterium*-associated IRIS model (1, 44, 45), particularly exhibiting inflamed lung even before T cell reconstitution (46). In contrast, human C-IRIS is known to affect any organs, including the CNS (47). Thus, we were prompted to examine the brain, as neurological dysfunction has a serious impact on patient morbidity and mortality (48). Here, we demonstrated that the pathology of C-IRIS induced with CnH99 shows a sharp contrast to *Mycobacterium*-associated IRIS pathology, as C-IRIS does not result in severe lung inflammation despite its lethal phenotype.

In our C-IRIS model, distinct pathological changes were observed in the brain. It is possible that, in C-IRIS, more dramatic leukocyte infiltration and brain damages could ultimately hamper and cause failure of essential motor functions of the mice. In C-IRIS mice, we found increased numbers of CD4$^+$ T cells, neutrophils, and microglia, as well as serious brain edema. Brain edema is caused by dysregulated water flux, which is controlled by aquaporins (AQPs). AQPs form a family of transmembrane channel proteins. Among 13 AQPs, only AQP4 is expressed in the brain (49, 50), where AQP4 is mainly expressed in astrocytes and plays a key role in regulating water flux in and out of the brain parenchyma (51, 52). In the CNS of *Cn*-infected mice, microglia may be activated in the vicinity of cryptococcal lesion, but the involvement of astrocytes were not studied for details (39). Overexpression of AQP4 induces brain edema (53), whereas AQP4 deletion reduces brain edema after acute water intoxication and ischemic stroke (54). We found heightened AQP4 expression in the brainstem of C-IRIS mice, as well as upregulation of *Aqp4* by IFNγ in an astrocyte cell line. We also demonstrated upregulation of *Aqp4* transcripts in an astrocyte cell line by IFNγ, as previously reported (55), as well as increased IFNγ protein levels in the brain of C-IRIS mice. Notably, no induction of AQP4 upregulation and brain edema were identified in mice received *Ifng*$^{-/-}$ CD4$^+$ T cells. Therefore, these results

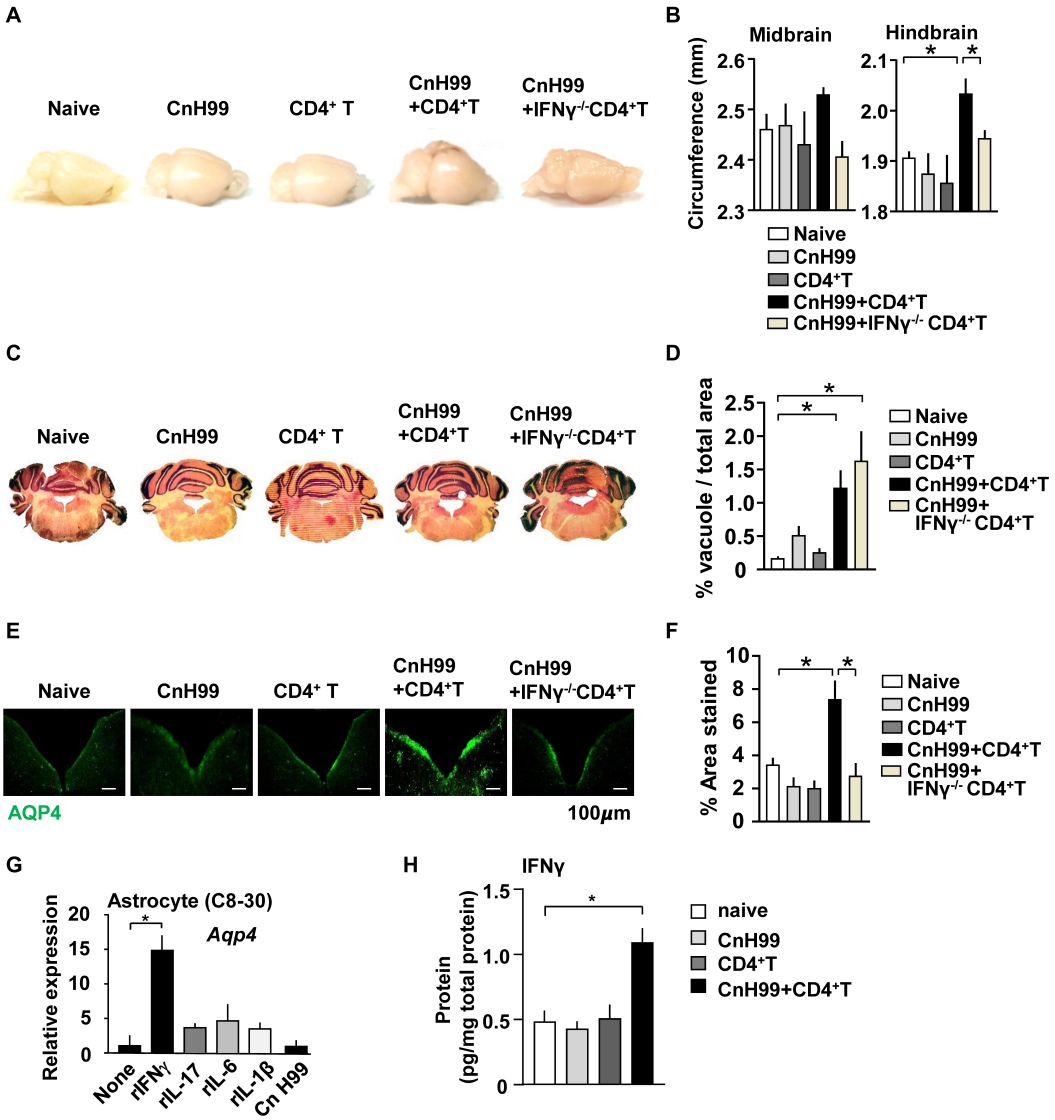

FIGURE 7 | Analyses of the brain in C-IRIS. **(A,B)** Representative images of brains from 5 groups of mice **(A)**. Quantitative analysis of tissue circumference of midbrain and hindbrain from 5 groups of mice **(B)**. *n = 5–8* mice/group. **(C,D)** Representative images of H&E stained hindbrain sections from 5 groups **(C)** and quantitative analysis of brain void spaces **(D)**. *n = 5* mice/group. **(E,F)** Representative images of AQP4-stained brain stem sections **(E)** and quantitative analysis of stained area **(F)**. *n = 3–5* mice/group. **(G)** Expression levels of *Aqp4* mRNA in the C8-30 astrocytes, treated with indicated recombinant cytokines (10 ng/ml for all) or CnH99 (MOI of 10) for 5 h. *n = 5* biological data-points/group. **(H)** Hindbrain IFNγ protein levels, evaluated with protein lysates of the hindbrain by ELISA. *n = 5–9* mice/group. Mice were treated with the protocol, indicated in **Supplementary Figure 1A** in all the *in vivo* experiments. The results are representatives from two independent experiments. One-way ANOVA and Tukey *post-hoc* test were used in **B**, **D**, **F**, and **H**. The Student's T test was used in **G**; $^*p < 0.05$.

bring a new hypothesis that brain-infiltrated Th1 cells inducing AQP4 and resulting brain edema, which has a lethal impact. The possible involvement of Th1 cell-induced AQP4 in astrocytes needs to be defined *in vivo* in future studies.

Multiple datasets from this study suggested the pathogenic involvement of IFNγ, particularly in the brain. Nevertheless, C-IRIS mice have not increased serum IFNγ levels (**Figure 2**). The result at least indicates that the impact of IFNγ in C-IRIS is not exerted at the systemic level, but the increase of local IFNγ is detrimental enough. The involvement of pathogenic factors, other than IFNγ but somehow linked to IFNγ, is also possible.

To assess the extent of the C-IRIS animal model reflecting human C-IRIS, more thorough studies are awaited. For example, in this study, we did not evaluate serum antibody profiles, which was suggested to be candidate biomarkers of human C-IRIS (56). We do not fully rule out the involvement of pulmonary complications and a possible pre-condition of heightened innate immunity prior to reconstitution in C-IRIS, but our results suggest that the mortality of C-IRIS mice is mainly attributed to brain damage that may seriously deteriorate essential vital brain function. This study also suggests a blockade of IFNγ in the brain may be therapeutically effective in C-IRIS and

nominates AQP4 as a novel target to ameliorate complications of intracranial pressure caused by C-IRIS. The interventions might be considered at the time of immune reconstitution, *e.g.,* antiretroviral therapy in HIV/AIDS. In conclusion, the mouse model of *Cn*—associated IRIS presented in this study provides a novel tool to unravel key mechanisms of pathogenesis.

DATA AVAILABILITY STATEMENT

All datasets generated for this study are included in the article/**Supplementary Material**. Raw data supporting the conclusions of this article will be made available by the authors without undue reservations.

ETHICS STATEMENT

The animal study was reviewed and approved by IACUC of Duke University; IACUC of University of Illinois-Urbana Champaign.

AUTHOR CONTRIBUTIONS

MI, WB, and NA optimized the initial experimental conditions. MI, YK, NA, WB, and EK generated the data for this publication. All authors participated in experimental designs and data analysis. YK, MI, and MS wrote the manuscript. WB and NA edited the manuscript. MI and MS equally contributed to design overall direction of the project.

FUNDING

Research reported in this publication was supported by NIH R01-AI136999 (MI) and R01-AI08810 and Duke Center for AIDS Research Micro Grant 5P30-AI064518 (MS).

ACKNOWLEDGMENTS

We thank Mary Clutter for helping with sample isolation and analysis. We also thank Duke Cancer Institute (DCI) Microscopy and Flow Cytometry core facilities.

SUPPLEMENTARY MATERIAL

The Supplementary Material for this article can be found online at: https://www.frontiersin.org/articles/10.3389/fimmu.2020.529219/full#supplementary-material

REFERENCES

1. Aggarwal N, Barclay W, Shinohara ML. Understanding mechanisms underlying the pathology of immune reconstitution inflammatory syndrome (IRIS) by using animal models. *Curr Clin Microbiol Rep*. (2018) 5:201–9. doi: 10.1007/s40588-018-0099-5
2. Elston JW, Thaker H. Immune reconstitution inflammatory syndrome. *Int J STD AIDS*. (2009) 20:221–4. doi: 10.1258/ijsa.2008.008449
3. Gupta AO, Singh N. Immune reconstitution syndrome and fungal infections. *Curr Opin Infect Dis*. (2011) 24:527–33. doi: 10.1097/QCO.0b013e32834ab20a
4. Longley N, Harrison TS, Jarvis JN. Cryptococcal immune reconstitution inflammatory syndrome. *Curr Opin Infect Dis*. (2013) 26:26–34. doi: 10.1097/QCO.0b013e32835c21d1
5. Meintjes G, Scriven J, Marais S. Management of the immune reconstitution inflammatory syndrome. *Curr HIV/AIDS Rep*. (2012) 9:238–50. doi: 10.1007/s11904-012-0129-5
6. Haddow LJ, Colebunders R, Meintjes G, Lawn SD, Elliott JH, Manabe YC, et al. Cryptococcal immune reconstitution inflammatory syndrome in HIV-1-infected individuals: proposed clinical case definitions. *Lancet Infect Dis*. (2010) 10:791–802. doi: 10.1016/S1473-3099(10)70170-5
7. Boulware DR, Meya DB, Bergemann TL, Wiesner DL, Rhein J, Musubire A, et al. Clinical features and serum biomarkers in HIV immune reconstitution inflammatory syndrome after cryptococcal meningitis: a prospective cohort study. *PLoS Med*. (2010) 7:e1000384. doi: 10.1371/journal.pmed.1000384
8. Muller M, Wandel S, Colebunders R, Attia S, Furrer H, Egger M, et al. Immune reconstitution inflammatory syndrome in patients starting antiretroviral therapy for HIV infection: a systematic review and meta-analysis. *Lancet Infect Dis*. (2010) 10:251–61. doi: 10.1016/S1473-3099(10)70026-8
9. Bowen LN, Smith B, Reich D, Quezado M, Nath A. HIV-associated opportunistic CNS infections: pathophysiology, diagnosis and treatment. *Nat Rev Neurol*. (2016) 12:662–74. doi: 10.1038/nrneurol.2016.149
10. Sun HY, Singh N. Immune reconstitution inflammatory syndrome in non-HIV immunocompromised patients. *Curr Opin Infect Dis*. (2009) 22:394–402. doi: 10.1097/QCO.0b013e32832d7aff
11. Husain S, Wagener MM, Singh N. Cryptococcus neoformans infection in organ transplant recipients: variables influencing clinical characteristics and outcome. *Emerg Infect Dis*. (2001) 7:375–81. doi: 10.3201/eid0703.010302
12. Gundacker ND, Jordan SJ, Jones BA, Drwiega JC, Pappas PG. Acute cryptococcal immune reconstitution inflammatory syndrome in a patient on natalizumab. *Open Forum Infect Dis*. (2016) 3:ofw038. doi: 10.1093/ofid/ofw038
13. Singh N, Perfect JR. Immune reconstitution syndrome and exacerbation of infections after pregnancy. *Clin Infect Dis*. (2007) 45:1192–9. doi: 10.1086/522182
14. Beeson PB. Cryptococcic meningitis of nearly sixteen years' duration. *AMA Arch Intern Med*. (1952) 89:797–801. doi: 10.1001/archinte.1952.00240050111008
15. Jansson L, Holmdahl R. Estrogen-mediated immunosuppression in autoimmune diseases. *Inflamm Res*. (1998) 47:290–301. doi: 10.1007/s000110050332
16. Ely EW, Peacock JE Jr., Haponik EF, Washburn RG. Cryptococcal pneumonia complicating pregnancy. *Medicine (Baltimore)*. (1998) 77:153–67. doi: 10.1097/00005792-199805000-00001
17. Kiggundu R, Rhein J, Meya DB, Boulware DR, Bahr NC. Unmasking cryptococcal meningitis immune reconstitution inflammatory syndrome in pregnancy induced by HIV antiretroviral therapy with postpartum paradoxical exacerbation. *Med Mycol Case Rep*. (2014) 5:16–9. doi: 10.1016/j.mmcr.2014.05.001
18. Boulware DR, Bonham SC, Meya DB, Wiesner DL, Park GS, Kambugu A, et al. Paucity of initial cerebrospinal fluid inflammation in cryptococcal meningitis is associated with subsequent immune reconstitution inflammatory syndrome. *J Infect Dis*. (2010) 202:962–70. doi: 10.1086/655785
19. Neal LM, Xing E, Xu J, Kolbe JL, Osterholzer JJ, Segal BM, et al. CD4(+) T cells orchestrate lethal immune pathology despite fungal clearance during

cryptococcus neoformans meningoencephalitis. *mBio*. (2017) 8:e01415-17. doi: 10.1128/mBio.01415-17
20. Antonelli LR, Mahnke Y, Hodge JN, Porter BO, Barber DL, Dersimonian R, et al. Elevated frequencies of highly activated CD4+ T cells in HIV+ patients developing immune reconstitution inflammatory syndrome. *Blood*. (2010) 116:3818–27. doi: 10.1182/blood-2010-05-285080
21. Mahnke YD, Greenwald JH, Dersimonian R, Roby G, Antonelli LR, Sher A, et al. Selective expansion of polyfunctional pathogen-specific CD4(+) T cells in HIV-1-infected patients with immune reconstitution inflammatory syndrome. *Blood*. (2012) 119:3105–12. doi: 10.1182/blood-2011-09-380840
22. Bicanic T, Meintjes G, Rebe K, Williams A, Loyse A, Wood R, et al. Immune reconstitution inflammatory syndrome in HIV-associated cryptococcal meningitis: a prospective study. *J Acquir Immune Defic Syndr*. (2009) 51:130–4. doi: 10.1097/QAI.0b013e3181a56f2e
23. Hsu JL, Ruoss SJ, Bower ND, Lin M, Holodniy M, Stevens DA. Diagnosing invasive fungal disease in critically ill patients. *Crit Rev Microbiol*. (2011) 37:277–312. doi: 10.3109/1040841X.2011.581223
24. Tani N, Rahnasto-Rilla M, Wittekindt C, Salminen KA, Ritvanen A, Ollakka R, et al. Antifungal activities of novel non-azole molecules against S. cerevisiae and C. albicans. *Eur J Med Chem*. (2012) 47:270–7. doi: 10.1016/j.ejmech.2011.10.053
25. Litvintseva AP, Kestenbaum L, Vilgalys R, Mitchell TG. Comparative analysis of environmental and clinical populations of *Cryptococcus neoformans*. *J Clin Microbiol*. (2005) 43:556–64. doi: 10.1128/JCM.43.2.556-564.2005
26. doi: 10.1128/cmr.8.4.515-548.1995Mitchell TG, Perfect JR. Cryptococcosis in the era of AIDS–100 years after the discovery of Cryptococcus neoformans. *Clin Microbiol Rev*. (1995) 8:515–48.
27. Rinaldi MG, Drutz DJ, Howell A, Sande MA, Wofsy CB, Hadley WK. Serotypes of *Cryptococcus neoformans* in patients with AIDS. *J Infect Dis*. (1986) 153:642. doi: 10.1093/infdis/153.3.642
28. Shimizu RY, Howard DH, Clancy MN. The variety of *Cryptococcus neoformans* in patients with AIDS. *J Infect Dis*. (1986) 154:1042. doi: 10.1093/infdis/154.6.1042
29. Sherman F. Getting started with yeast. *Methods Enzymol*. (1991) 194:3–21. doi: 10.1016/0076-6879(91)94004-v
30. Hogmalm A, Bry M, Strandvik B, Bry K. IL-1beta expression in the distal lung epithelium disrupts lung morphogenesis and epithelial cell differentiation in fetal mice. *Am J Physiol Lung Cell Mol Physiol*. (2014) 306:L23–34. doi: 10.1152/ajplung.00154.2013
31. Wiesner DL, Boulware DR. Cryptococcus-related immune reconstitution inflammatory syndrome(IRIS): pathogenesis and its clinical implications. *Curr Fungal Infect Rep*. (2011) 5:252–61. doi: 10.1007/s12281-011-0064-8
32. Grant PM, Komarow L, Lederman MM, Pahwa S, Zolopa AR, Andersen J, et al. Elevated interleukin 8 and T-helper 1 and T-helper 17 cytokine levels prior to antiretroviral therapy in participants who developed immune reconstitution inflammatory syndrome during ACTG A5164. *J Infect Dis*. (2012) 206:1715–23. doi: 10.1093/infdis/jis604
33. Maziarz EK, Perfect JR. Cryptococcosis. *Infect Dis Clin North Am*. (2016) 30:179–206. doi: 10.1016/j.idc.2015.10.006
34. Meya DB, Manabe YC, Boulware DR, Janoff EN. The immunopathogenesis of cryptococcal immune reconstitution inflammatory syndrome: understanding a conundrum. *Curr Opin Infect Dis*. (2016) 29:10–22. doi: 10.1097/QCO.0000000000000224
35. Tan DB, Yong YK, Tan HY, Kamarulzaman A, Tan LH, Lim A, et al. Immunological profiles of immune restoration disease presenting as mycobacterial lymphadenitis and cryptococcal meningitis. *HIV Med*. (2008) 9:307–16. doi: 10.1111/j.1468-1293.2008.00565.x
36. Schmued LC, Albertson C, Slikker W Jr. Fluoro-Jade: a novel fluorochrome for the sensitive and reliable histochemical localization of neuronal degeneration. *Brain Res*. (1997) 751:37–46. doi: 10.1016/s0006-8993(96)01387-x
37. Ito H, Yamamoto N, Arima H, Hirate H, Morishima T, Umenishi F, et al. Interleukin-1beta induces the expression of aquaporin-4 through a nuclear factor-kappaB pathway in rat astrocytes. *J Neurochem*. (2006) 99:107–18. doi: 10.1111/j.1471-4159.2006.04036.x
38. Sun L, Li M, Ma X, Feng H, Song J, Lv C, et al. Inhibition of HMGB1 reduces rat spinal cord astrocytic swelling and AQP4 expression after oxygen-glucose deprivation and reoxygenation via TLR4 and NF-kappaB signaling in an IL-6-dependent manner. *J Neuroinflammation*. (2017) 14:231. doi: 10.1186/s12974-017-1008-1
39. Eschke M, Piehler D, Schulze B, Richter T, Grahnert A, Protschka M, et al. A novel experimental model of *Cryptococcus neoformans*-related immune reconstitution inflammatory syndrome (IRIS) provides insights into pathogenesis. *Eur J Immunol*. (2015) 45:3339–50. doi: 10.1002/eji.201545689
40. Decken K, Kohler G, Palmer-Lehmann K, Wunderlin A, Mattner F, Magram J, et al. Interleukin-12 is essential for a protective Th1 response in mice infected with *Cryptococcus neoformans*. *Infect Immun*. (1998) 66:4994–5000. doi: 10.1128/iai.66.10.4994-5000.1998
41. Morrow CA, Lee IR, Chow EW, Ormerod KL, Goldinger A, Byrnes EJ III, et al. A unique chromosomal rearrangement in the Cryptococcus neoformans var. grubii type strain enhances key phenotypes associated with virulence. *mBio*. (2012) 3:e00310-11. doi: 10.1128/mBio.00310-11
42. Inoue M, Arikawa T, Chen YH, Moriwaki Y, Price M, Brown M, et al. T cells down-regulate macrophage TNF production by IRAK1-mediated IL-10 expression and control innate hyperinflammation. *Proc Natl Acad Sci USA*. (2014) 111:5295–300. doi: 10.1073/pnas.1321427111
43. Urai M, Kaneko Y, Ueno K, Okubo Y, Aizawa T, Fukazawa H, et al. Evasion of innate immune responses by the highly virulent *Cryptococcus gattii* by altering capsule glucuronoxylomannan structure. *Front Cell Infect Microbiol*. (2015) 5:101. doi: 10.3389/fcimb.2015.00101
44. Barber DL, Andrade BB, Mcberry C, Sereti I, Sher A. Role of IL-6 in *Mycobacterium avium*–associated immune reconstitution inflammatory syndrome. *J Immunol*. (2014) 192:676–82. doi: 10.4049/jimmunol.1301004
45. Barber DL, Mayer-Barber KD, Antonelli LR, Wilson MS, White S, Caspar P, et al. Th1-driven immune reconstitution disease in Mycobacterium avium-infected mice. *Blood*. (2010) 116:3485–93. doi: 10.1182/blood-2010-05-286336
46. Barber DL, Andrade BB, Sereti I, Sher A. Immune reconstitution inflammatory syndrome: the trouble with immunity when you had none. *Nat Rev Microbiol*. (2012) 10:150–6. doi: 10.1038/nrmicro2712
47. Shelburne SA III, Hamill RJ, Rodriguez-Barradas MC, Greenberg SB, Atmar RL, Musher DW, et al. Immune reconstitution inflammatory syndrome: emergence of a unique syndrome during highly active antiretroviral therapy. *Medicine (Baltimore)*. (2002) 81:213–27. doi: 10.1097/00005792-200205000-00005
48. Mccombe JA, Auer RN, Maingat FG, Houston S, Gill MJ, Power C. Neurologic immune reconstitution inflammatory syndrome in HIV/AIDS: outcome and epidemiology. *Neurology*. (2009) 72:835–41. doi: 10.1212/01.wnl.0000343854.80344.69
49. Zelenin S, Gunnarson E, Alikina T, Bondar A, Aperia A. Identification of a new form of AQP4 mRNA that is developmentally expressed in mouse brain. *Pediatr Res*. (2000) 48:335–9. doi: 10.1203/00006450-200009000-00012
50. Vella J, Zammit C, Di Giovanni G, Muscat R, Valentino M. The central role of aquaporins in the pathophysiology of ischemic stroke. *Front Cell Neurosci*. (2015) 9:108. doi: 10.3389/fncel.2015.00108
51. Potokar M, Stenovec M, Jorgacevski J, Holen T, Kreft M, Ottersen OP, et al. Regulation of AQP4 surface expression via vesicle mobility in astrocytes. *Glia*. (2013) 61:917–28. doi: 10.1002/glia.22485
52. Yukutake Y, Yasui M. Regulation of water permeability through aquaporin-4. *Neuroscience*. (2010) 168:885–91. doi: 10.1016/j.neuroscience.2009.10.029
53. Yang B, Zador Z, Verkman AS. Glial cell aquaporin-4 overexpression in transgenic mice accelerates cytotoxic brain swelling. *J Biol Chem*. (2008) 283:15280–6. doi: 10.1074/jbc.M801425200
54. Manley DM, Mccomb ME, Perreault H, Donald LJ, Duckworth HW, O'neil JD. Secondary structure and oligomerization of the E. coli

glycerol facilitator. *Biochemistry*. (2000) 39:12303–11. doi: 10.1021/bi000703t

55. Asai H, Kakita H, Aoyama M, Nagaya Y, Saitoh S, Asai K. Diclofenac enhances proinflammatory cytokine-induced aquaporin-4 expression in cultured astrocyte. *Cell Mol Neurobiol*. (2013) 33:393–400. doi: 10.1007/s10571-013-9905-z
56. Yoon HA, Nakouzi A, Chang CC, Kuniholm MH, Carreno LJ, Wang T, et al. Association between plasma antibody responses and risk for Cryptococcus-associated immune reconstitution inflammatory syndrome. *J Infect Dis*. (2019) 219:420–8. doi: 10.1093/infdis/jiy447

Conflict of Interest: The authors declare that the research was conducted in the absence of any commercial or financial relationships that could be construed as a potential conflict of interest.